Composite Structures 179 (2017) 245–257

Contents lists available at ScienceDirect

Composite Structures

journal homepage: www.elsevier.com/locate/compstruct

An analytical model for the ballistic performance of ultra-high molecular weight polyethylene composites

Tye Langston

Naval Surface Warfare Center, 110 Vernon Avenue, Panama City, FL 33407, USA

ARTICLE INFO

Article history:
Received 3 November 2016
Revised 1 March 2017
Accepted 18 July 2017
Available online 22 July 2017

ABSTRACT

Ultra-high molecular weight polyethylene (UHMWPE) fibers are often used in ballistic armor due to their excellent strength, stiffness, strain to failure, and low density. Despite applicability and growing usage, designing UHMWPE armor systems is challenging. The unique properties of their fibers and matrix materials cause UHMWPE composites to behave differently than other composites. To realize their potential and effectively apply them to armor applications, it is important to understand their failure mechanisms and model their performance without the aid of complicated computer models. This study focuses on understanding their energy absorption and through-thickness failure mechanisms, as well as developing an analytical model to predict ballistic performance. Energy absorption was considered from fiber tensile strain, delamination between layers, matrix cracking, acceleration of the composite mass, and shear failure. Tensile failures from the formation of the deformation cone and out-of-plane compression were considered, as well as shear failure. The analytical formulation predicts the amount of energy absorbed by each mechanism, ballistic limit, duration of the impact event, through-thickness failure distance, and residual velocity. The results were compared with experimental data and good correlation was observed for a range of projectile masses and diameters, as well as composite thicknesses.

Published by Elsevier Ltd.

1. Introduction

One of the primary focuses of modern ballistic armor design, along with improved ballistic resistance, is reduced weight. Although protection can be achieved for most ballistic threats, it is not practical unless it is at an operationally useful weight. And further reducing weight even below the operational requirements is almost always preferred. Heavy personal armor systems slow down the wearer and are often just not worn due to their awkwardness and discomfort. Heavy vehicle armor systems affect maneuverability, fuel economy, and overall performance in general.

High performance fibers have received a lot of attention for ballistic protection. They possess exceptional properties that are particularly applicable to armor, such as high strength, high stiffness and low density. Some of the more notable high strength fibers include *para*-aramid (Kevlar®, Twaron®); poly-pyridobisimidazole (M5®); poly-benzobis-oxazole (Zylon®); ultra-high molecular weight polyethylene (Dyneema® and Spectra®); and carbon. While all of these fibers have some advantages in comparison to the others, UHMWPE fibers offer the lowest density, while maintaining exceptionally high tensile strength and one of the highest failure strains [1–7]. Furthermore, in ballistic protection, dynamic properties are of even more importance than static ones. Russell et al. [6] evaluated UHMWPE fibers, yarns and composites at different strain rates, and found very little variation in failure strength and strain within the strain rate range of 10^{-1}–10^{3} s^{-1}. This was echoed by Huang et al. [1], who observed no variation in failure stress and minimal strain variation at strain rates of 300 and 700 s^{-1}. For these reasons, UHMWPE is often selected in modern armor designs. As such, this current study specifically focuses on analytically modeling the ballistic resistance and energy absorption of UHMWPE composite armor.

Of course, a composite is composed of more than just the fibers. The matrix also contributes to the overall performance, albeit in different ways. While the fibers are primarily responsible for composite strength, the matrix plays a larger role in interlaminar shear, delamination, and generally maintaining fibers in their relative positions. The matrix volume fraction used in UHMWPE composites is often less than 20%, which is very low in relation to some other composite types [6,8]. The matrix materials used with UHMWPE fibers are often very tough. Dyneema ® HB26, for example, utilizes a polyurethane matrix material.

While the benefits of UHMWPE composites in armor applications are difficult to argue against, designing a system for ballistic

E-mail address: tye.langston@navy.mil

http://dx.doi.org/10.1016/j.compstruct.2017.07.074
0263-8223/Published by Elsevier Ltd.

Notation

A_b	Area of accelerated composite material
a_n	Proportion of each fiber orientation of the total fiber content
A_{ql}	Quasi-lemniscate area reduction factor
c_p	Plastic wave speed
c_T	Transverse wave speed
dc	Projectile deceleration
d_f	Fiber diameter
dt	Time step
d_P	Projectile diameter
$E_{Acceleration}$	Energy absorbed in accelerating composite mass
E_c	Composite modulus
$E_{Cracking}$	Energy absorbed in matrix cracking
$E_{Delamination}$	Energy absorbed in delamination
E_f	Fiber modulus
$E_{KE,Proj}$	Projectile kinetic energy
E_m	Matrix modulus
E_{Shear}	Energy absorbed in composite shear failure
$E_{Tensile}$	Energy absorbed in tensile strain
E_{Total}	Total energy absorbed
F	Projectile contact force
Fp	Contact force from projectile and sheared composite material mass at its tip
G_c	Combined critical strain energy release rate
G_I	Mode I critical strain energy release rate
G_{II}	Mode II critical strain energy release rate
h_c	Composite thickness
h_L	Layer thickness
L_T	Length of target edge in a finite sized target
m_p	Projectile mass
N_{IF}	Number of remaining interfaces in the portion of the composite that had not yet failed
N_L	Number of layers remaining that have not failed
N_{SP}	Number of layers failed in shear
N_T	Number of layers failed in tension
N_{TC}	Number of layers failed in transverse tensile cracking
P_{IF}	Fraction of the interfaces that delaminate
P_m	Percentage of total matrix cracking
r_p	Radius plastic wave has reached
r_T	Radius the transverse wave has reached
S_p	Distance projectile has traveled after contacting composite
S_{SP}	Composite through-thickness shear strength
V	poisson's ratio
v	Velocity
V_f	Fiber volume fraction
v_o	Initial projectile velocity
β_θ	Krenchel's composite reinforcing efficiency
ε_c	Tensile strain in a ply from compression
$\varepsilon_{f,f}$	Fiber dynamic failure strain
$\varepsilon_{m,f}$	Matrix dynamic failure strain
$\varepsilon_{p,f}$	Ply dynamic failure strain
ε_p	Composite strain at yield
ε_t	Tensile strain in a ply from cone formation
ρ_c	Composite density
ρ_f	Fiber density
ρ_m	Matrix density
σ_c	Compressive stress under projectile
$\sigma_{f,f}$	Fiber dynamic failure strength
$\sigma_{m,f}$	Matrix dynamic failure strength
σ_{SP}	Shear plugging stress
σ_t	Tensile stress in ply
θ_f	Fiber orientation angle
Θ	Composite bending angle

protection is not straight forward. The response of a UHMWPE composite to an impacting projectile is a very complicated process, with many energy absorption and failure mechanisms coming into play, such as tensile strain, out of plane compression, delamination and acceleration of material mass. While these individual aspects of composite behavior are all understood on some level, it is difficult to combine them into an accurate analytical model that can be used to predict ballistic performance and aid in armor design. Furthermore, the unique properties of the UHMWPE fibers and the associated matrix materials may lead to the failure processes of these composites to be different than those of other fibrous composite types. This paper presents a complete model for UHMWPE ballistic response, in terms of energy absorption, though-thickness failure, ballistic limit, residual velocity, and the duration of the event, and compares its predictions against published experimental data.

2. Analytical model

2.1. Calculation methodology

The current model allows for the reduction of a projectile's kinetic energy by balancing it with the various energy absorption mechanisms activated in the composite. Five sources of energy absorption were considered: fiber tensile strain, delamination between layers, matrix cracking, acceleration of the composite mass, and shear failure of the composite. The total energy lost by the projectile during impact equals the total amount absorbed by the different composite energy absorption mechanisms:

$$E_{Total} = E_{KE,Proj} + E_{Tensile} + E_{Delamination} + E_{Acceleration} + E_{Cracking} + E_{Shear} \quad (1)$$

At velocities below the ballistic limit, all of the projectile kinetic energy is absorbed by the composite and the projectile velocity is reduced to zero. However, when the initial kinetic energy of the projectile exceeds the ballistic limit of the target composite, failure occurs before all energy is absorbed and the projectile retains some residual velocity. Therefore, in addition to the reduction of the projectile kinetic energy by composite energy absorption, the model also considered through-thickness failure distance of the composite. The impact event was considered to be concluded when either the full amount of the initial projectile kinetic energy was absorbed by the composite, or when the composite failed through its entire thickness.

Two modes were considered for through-thickness failure: tensile failure (front face) and shear plugging failure. The front face tension used for layer failure determination was a combination of the tensile strain from the formation of the deformation cone and the strain that arose from compression directly under the projectile. Transverse cracking failure at the rear face was also initially considered but was not found to play a significant role. Although this type of failure is important in other composite types, such as in carbon/epoxy [9], neither the model results nor literature reviews indicated that it plays a significant role in UHMWPE failure. Furthermore, other researchers have demonstrated that UHMWPE composite failure occurs primarily from front to back [10–13].

Other types of general material failures exist in this type of composite, such as delamination and matrix cracking, and were

considered with regard to energy absorption. However, tensile and shear plugging were the only ones that were considered to effectively reduce the composite thickness and allow projectile penetration. Each failure mode proceeded layer by layer through the composite until either the projectile's kinetic energy was reduced to zero, or the total number of combined failed layers was greater than the overall number of layers in the composite. Shear plugging and tensile failure both proceeded from the front (impact side) of the composite plate and they were mutually exclusive. The total number of failed layers is equal to the sum of the number of layers failed by tension and shear:

$$N_{Total} = N_{Tensile} + N_{Shear} \tag{2}$$

Layer failure was determined by comparing the instantaneous composite tensile strain and shear stresses against their maximum values as the projectile progressed through the composite. In the case of tensile failure, if the total tensile strain was determined to be greater than the ply failure strain when it reached the end of a layer, that layer was considered to have failed. Because the fibers considered in this effort have higher failure strains than the matrix, the ply failure strain, $\varepsilon_{p,f}$, is equal to the fiber failure strain. Total tensile strain included components from compression under the projectile, ε_c, as described by Attwood et al. [14], as well as tensile strain resulting from deformation, ε_t. Thus,

If $(S_{p,i} \geqslant nh_L$ and $(\varepsilon_{t,i} + \varepsilon_{c,i}) \geqslant \varepsilon_{p,f}$, $N_{T,i} = n,)$ where S_p is the distance the projectile has traveled in the composite, n is the number of layer interfaces that the projectile has reached, and h_L is the layer height.

The approach for shear plugging is similar. Based on the projectile contact force and tip diameter, if the projectile reaches an interface and the shear stress generated is enough to fail that ply, that layer is considered to have failed. Therefore, if $(S_{p,i} \geqslant nh_L$ and $\sigma_{SP,i} \geqslant S_{SP}$, $N_{SP,i} = n,)$ where σ_{SP} is the shear plugging stress in the ply and S_{SP} is the composite through-thickness shear strength. N_{SP} is the number of layers failed in shear. It should be noted that if both tensile and shear failure criteria where met, the number of failed layers was only allowed to increase by one.

The model formulation was based on repeating calculations at discrete time intervals, and included the following assumptions:

1. The composite is a flat plate.
2. A 0/90° layup.
3. The projectile strikes the composite at normal incidence.
4. No mass is lost from the projectile.
5. The projectile is cylindrical.
6. The projectile motion is constant across each discreet time interval.

For each time interval, the energy absorption was calculated for the various different energy absorption mechanisms using the motion of the projectile and the force it imposed upon the composite. The projectile velocity, deceleration, distance traveled, and contact force for the ith time interval can be expressed as:

Velocity:

$$v_i = \sqrt{v_o^2 - \frac{2E_{Total,i}}{m_p}} \tag{3}$$

Deceleration:

$$dc_i = \frac{v_{i-1} - v_i}{dt} \tag{4}$$

Distance Traveled:

$$S_{p,i} = v_{i-1}dt - \frac{1}{2}dc_i dt^2 \tag{5}$$

Contact Force:

$$F_i = m_p dc_i \tag{6}$$

where v_o is the initial projectile velocity, dt is the time step and m_p is the projectile mass. The values for the first iteration were attained by initially assuming the amount of energy absorbed in the first step and then iterating until that value had converged.

2.2. Energy absorption mechanisms and failure modes

2.2.1. Tensile strain from cone formation

After projectile impact, but before complete composite failure, the composite material deforms in response to the projectile force. Smith et al. [15] and Roylance et al. [16] mathematically described a similar deformation process in yarns subjected to transverse impact. They argued that immediately after impact, a series of waves propagate outward at different speeds. The first elastic wave is followed by a series of longitudinal strain wavelets, and then finally a transverse wave. The strain wavelets (plastic waves) cause material to flow inwards towards the point of impact, leading to energy absorption through tensile strain. The slower transverse wave follows in the wake of the plastic wave front. After passage of the plastic wave, the tensile strain no longer changes, but the material moves in a transverse direction, parallel to the projectile. As the projectile and moving composite mass slow down and stop, the tensile strain at the base of the cone will also reduce. Fig. 1 describes this failure theory.

The speed of the plastic wave that governs strain is dependent on the density and the instantaneous slope of the tensile stress–strain curve at yield (ε_p) [15,17]:

$$c_p = \sqrt{\frac{1}{\rho}\left(\frac{d\sigma}{d\epsilon}\right)_{\epsilon=\epsilon_p}} \tag{7}$$

The dynamic stress–strain curves for UHMWPE fiber and yarn have been described by Russell et al. [6]. In their experiments, they found very little variation in failure strength and strain within the strain rate range of 10^{-1}–10^{3} s^{-1}. It was also apparent that at strain rates over 10^{0} s^{-1}, the fibers exhibited simple Hookean stress–strain curves. By applying Eq. (7) to Russell et al.'s data, a fiber wave speed of 11,350 m/s was attained (or 10,325 m/s for a unidirectional composite). This is similar to what was reported by Chocron et al. [18] and Hudspeth et al. [19] Huang et al. [1] also evaluated UHMWPE fiber bundles at different strain rates (300 and 700 s^{-1}). Like Russell et al., they showed minimal variation in failure stress and strain at different strain rates. Their reported failure stress values were similar to those reported by Russell et al. However, they reported higher failure strains. Russell et al. suggested that this difference was due to the test methods, as Russell et al. measured the elongation of a gauge length on the specimen and Huang et al. used the relative displacement of the grips, which doesn't account for any slip that may occur. The transverse wave velocity can be related to the plastic wave velocity and the plastic strain in the composite [15]:

$$c_T = c_p\sqrt{\frac{\varepsilon_p}{(1+\varepsilon_p)}} \tag{8}$$

Although the formulation described by Smith et al. and Roylance et al. was initially done for yarns, it has been meaningfully applied to impact of other types of fibrous composite plates. Refer to Naik et al. [17] for an example with E-glass/epoxy, as well as Utomo & Ernst [20]. Indeed, this type of deformation described by these equations has also been observed experimentally in composite laminates subjected to ballistic impact. Karthikeyan et al. [10] described the presence of a "travelling hinge" that emanated

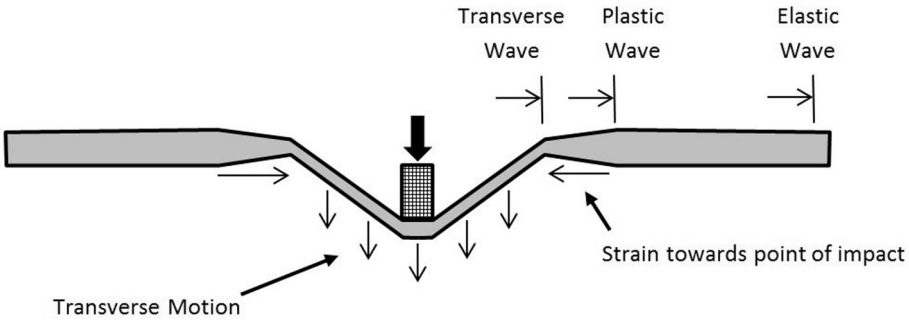

Fig. 1. Description of strain, plastic wave and transverse wave in composite under ballistic loading.

outward from the point of impact during ballistic testing of carbon fiber and UHMWPE laminated plates. Furthermore, ballistic UHMWPE fabric is usually not woven. It consists of layers of unidirectional prepreg fibers, so weave architecture is not a concern in extending the Smith et al. and Roylance et al. yarn model to a composite.

The strain energy absorbed by this outward travelling plastic wave depends on the volume of the material subjected to the strain, as well as the orientation of the fibers. The current analysis considered a laminate with alternating 0/90 degree plies, which leads to some anisotropy. This is a common layup for UHMWPE composites. To account for fiber orientation, the Krenchel composite efficiency factor was included in the calculations for the composite modulus [18–20]. This approach helps to avoid extensive classical composite analysis computations, but it is an approximation. For composites containing high volume fractions of high-stiffness fibers, such as UHMWPE composites, it is believed to give reasonable estimates [18].

Krenchel's reinforcing efficiency can be found by [21–23]:

$$\beta_\theta = \sum a_n \cos^4 \theta_f \tag{9}$$

where a_n is the proportion of each fiber orientation of the total fiber content and θ_f is the fiber orientation angle. Using this efficiency factor, the approximate composite modulus can be found from a modified rule of mixtures [21,23,24]:

$$E_c = \beta_\theta E_f V_f + E_m(1 - V_f) \tag{10}$$

where E_f and E_m are the modulus for the fiber and matrix, respectively, and V_f is the fiber volume fraction. The strained region of the composite travels outward at the plastic wave speed, with the strain being highest at the point of impact and diminishing with increasing diameter. From Smith et al. [15], the projectile velocity can be related to the strain (ε_t):

$$v = c_p \sqrt{\varepsilon_t(1+\varepsilon_t) - \left[\sqrt{\varepsilon_t(1+\varepsilon_t)} - \varepsilon_t\right]^2} \tag{11}$$

Furthermore, through experiments on woven fabric laminated plates Naik et al. [25] and Wu et al. [26] showed that although the shape of the deformation cone base is somewhat circular, it is not precisely so. Instead, it is quasi-lemniscate. This is primarily due to the anisotropy resulting from fiber orientation in alternating plies. It was observed that the protrusion tends to grow more along the fiber directions than in others. This damage pattern has been consistently observed in UHMWPE, carbon, and E-glass composites [10,25,26]. Fig. 2 shows the transient damage area of a UHMWPE composite acquired through dynamic shadow moiré interference fringe patterns [10]. Therefore, the area of the cone base in the model was modified by a quasi-lemniscate area reduction factor, A_{ql}, of 0.9, similar to that used by Naik et al. [25]. Another important point is that not only does the area of the base deviate from circular, but the strain profile is also changed with the strain being higher along the fiber directions and lower in between. With respect to strain, an approximation was made and it was assumed to be constant around the circumference of the protrusion.

The affected composite volume depends not only on the distance the plastic wave has reached, but also the effective thickness of the composite after failed layers have been accounted for. As layers of the composite fail by shear or tension, the effective thickness of the composite is reduced. These failed layers were no longer included in the tensile strain energy absorption calculations of the model because their fibers were severed and they had usually delaminated from the remaining composite. This approach is supported by the ballistic X-ray analyses done by Karthikeyan et al. (Fig. 4), which show extensive delamination and fiber failure as the projectile travels though UHMWPE and carbon fiber composites, leaving only the intact composite thickness to resist the projectile motion. Tensile Strain energy can be described as:

$$E_{Tensile} = \int_0^{\varepsilon} E_c\ \varepsilon\ d\varepsilon \cdot V \tag{12}$$

where V is the strained volume. Considering this from an incremental perspective, the volume depends on the area that is covered by the plastic wave progress in one increment and the actual remaining thickness of the composite after the failed layers are removed. Layer failure can occur by tension and shear, leaving the incremental volume to be:

$$V_i = \pi\left(r_{p,i}^2 - r_{p,i-1}^2\right) \cdot \left(h_c - N_{SP,i}h_L - N_{T,i}h_L\right) \tag{13}$$

where r_p is the radius the plastic wave has reached, h_c is the initial composite thickness, h_L is the layer thickness, N_{SP} is the number of layers failed in shear and N_T is the number of layers failed in tension. Integrating Eq. (12), using the strain that is appropriate for the current projectile velocity (from Eq. (11)), and applying the volume for the current increment leads to the expression for energy absorbed through tensile strain:

$$E_{Tensile} = .5\pi \sum E_c \varepsilon_{t,i}^2 \left(r_{p,i}^2 - r_{p,i-1}^2\right) \cdot \left(h_c - N_{SP,i}h_L - N_{T,i}h_L\right) \tag{14}$$

2.2.2. Tensile strain from compression under projectile

In addition to tensile strain from cone formation, another type of tensile strain occurs directly under the impacting body. This was first described by Woodward et al. [27] after performing indention studies on composites. They argued that the material under an indenter is confined by the surrounding material and unable to flow laterally when subjected to compressive stress. As the indenter depth increases, the stress below it increases until the plies closest to the indenter, which are strained the most, fail in tension. O'Masta et al. [8] and Attwood et al. [14] also argued that compressive stress leads to tensile stress in cross-ply lami-

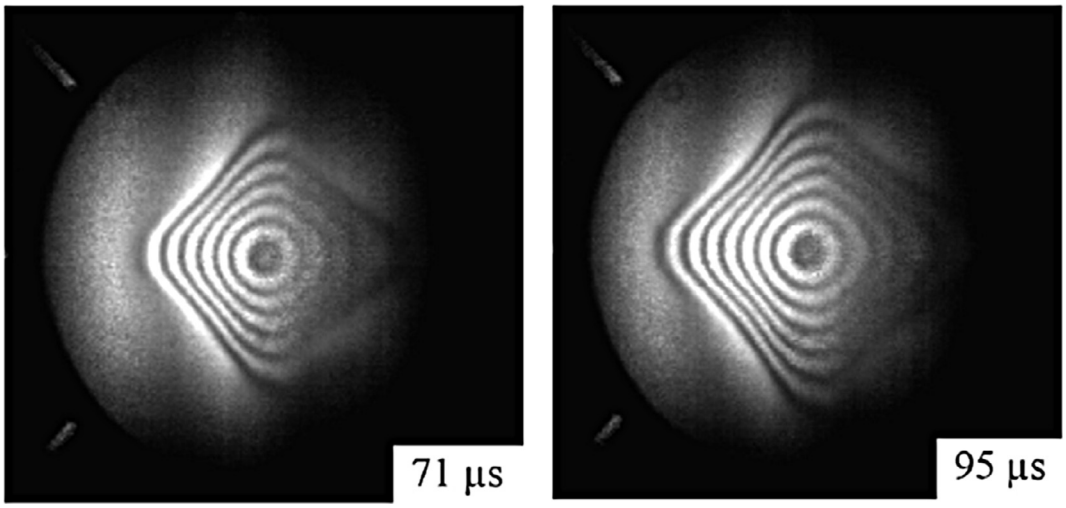

Fig. 2. UHMWPE (Dyneema® HB26) plate dynamic shadow moiré interference fringe patterns (from Karthikeyan et al. [10]);

nates subjected to ballistic impact. They hypothesized that this is due to shear-lag loading between plies with fibers in different directions. Attwood et al. [14] experimentally evaluated this failure concept and demonstrated the pressure sensitivity of Dyneema UHMWPE composites, showing that under compression, the material flows in the direction perpendicular to the fibers much more than in the fiber direction. Fig. 3 depicts this mode of failure.

The disproportional movement between the alternating plies creates additional tensile stress in the fibers, beyond that from the initial straining due to composite cone formation. The compressive stress under the projectile in the composite can be expressed as [22]:

$$\sigma_{c,i} = \frac{\sigma_{t,i}}{V}\left(\frac{E_f + E_m}{E_f}\right) \tag{15}$$

where σ_t is the tensile stress in the ply and V is the Poisson's ratio. E represents the Young's modulus for the fiber and matrix. By allowing σ_t to equal the ply tensile failure stress, the tensile strain in the ply from compression can be determined [14]:

$$\varepsilon_{c,i} = \frac{\sigma_{c,i}}{E_m}\left(1 - \frac{V^2 E_f}{E_f + E_m}\right) \tag{16}$$

A good approximation for the ply failure stress can be attained by considering the fiber failure strength, $\sigma_{f,f}$, matrix failure strength, $\sigma_{m,f}$, and fiber volume fraction, V_f, in the rule of mixtures. This strain is added to the maximum tensile strain resulting from cone formation to evaluate failure of each layer, which progresses from the impact side of the composite. The maximum cone strain is used because this type of failure occurs directly under the projectile where the cone strain maximum also occurs. While the tensile strain from compression plays an important role in through-thickness failure, the energy absorption from this mechanism is much smaller than that from the tensile strain due to cone formation because compression only occurs in a small area under the impacting body. Therefore, the energy absorption from this mechanism was assumed to be comparatively small and was not considered.

2.2.3. Delamination between layers

Through ballistic testing and cross-sectional analysis of failed targets, Gellert et al. [28] described the distribution of delaminations in the ballistic failure of glass/vinylester layered composites. They showed that the delamination zone took on a conical shape that expanded from approximately the projectile diameter on the strike face to a larger area on the rear of the failed plate. For relatively thick targets, they observed more of an hourglass distribution of delaminations. This is likely due to the bending stresses (tensile and compressive) that arise in the rigid glass/vinylester composite, which would be expected to be greater near the outer faces.

With respect to UHMWPE composites, researchers have noted extensive delamination during ballistic impact. Deka et al. [29] observed this both in ballistic testing and through a computer

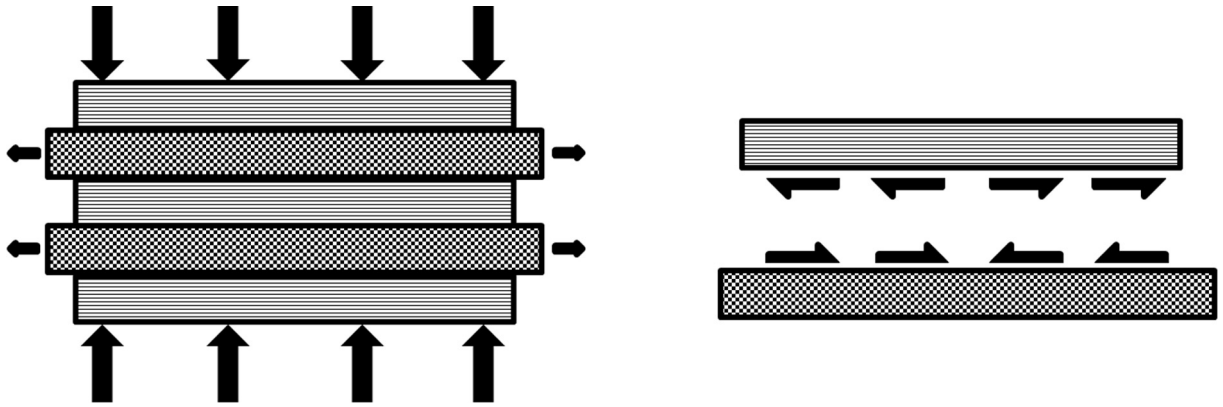

Fig. 3. Description of tensile stress under projectile due to compression.

model. Karthikeyan et al. [10] visually captured this process through X-ray analysis of ballistic tests. Fig. 4 shows some of their results. It can be seen that the delaminations reached all the way to the base of the composite deformation cone. In addition to the general delamination extent, another important observation that can be made from their work is that in these cases, the delaminated area is greater near the back of the composite than at the front. Thus, it appears that the delaminations of the UHMWPE composites follow a somewhat conical pattern (smaller in the front and larger in the back), similar to that described by Gellert et al. for glass/vinylester.

Considering the work of Gellert et al. [28], Deka et al. [29], and Karthikeyan et al. [10], the current analysis considered a delamination profile that grew outward with time and penetration depth. A connection was made between failure of the composite layers (shear or tensile) and the growth of the delaminations. Delaminations were only allowed to continue to grow in the composite region that had not failed by shear or tension. Once a layer failed, the delamination at the interface between it and the previously failed layer ceased to grow. Fig. 5 shows this approach, which leads to a conical delamination pattern.

The energy absorbed during delamination is dependent on the crack area and the strain energy release rate. Thus, the energy absorbed by delamination was taken to be:

$$E_{Delamination} = \sum \pi A_{ql} r_{T,i}^2 G_c N_{IF,i} P_{IF} \quad (17)$$

where G_c is the combined critical strain energy release rate, and N_{IF} is the number of remaining interfaces in the portion of the composite that had not yet failed. N_{IF} is determined by considering the distance the projectile has traveled through the composite (S_p) and the associated number of layers that have failed. Failed layers and their interfaces were no longer considered to contribute to the delamination energy. As shown in Fig. 4, not all of the interfaces delaminate and a fraction, P_{IF}, was used to represent the interfaces that do. A P_{IF} value of .08 was applied in the model based on inspection of the X-ray images provided by Karthikeyan et al. [10]. From their work, the fraction of interfaces that delaminated was similar for both the HB26 and HB50 grades of Dyneema. And similar to Naik [17], the quasi-lemnescate area reduction factor was applied to the delamination area to account for the non-circular shape of the delamination area due to fiber direction anisotropy.

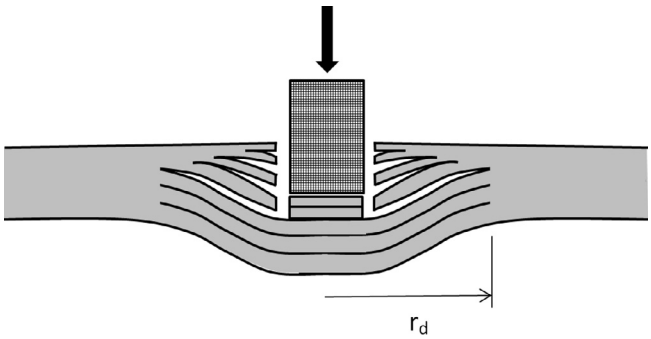

Fig. 5. Description of delamination approach.

The strain energy release rate for delamination was assumed to be from mixed mode I and II failure, as described by Nguyen et al. [11] and Grujicic et al. [13]. Mode I and II values for UHMWPE have been presented by Grujicic et al. [13], which were determined through a combination of finite element analysis and open-literature data. In addition, others have experimentally measured these properties for UHMWPE composites, providing reasonable agreement with Grujicic et al. [13]. Lassig et al. [30] have recently published experimental determinations of mode I values and

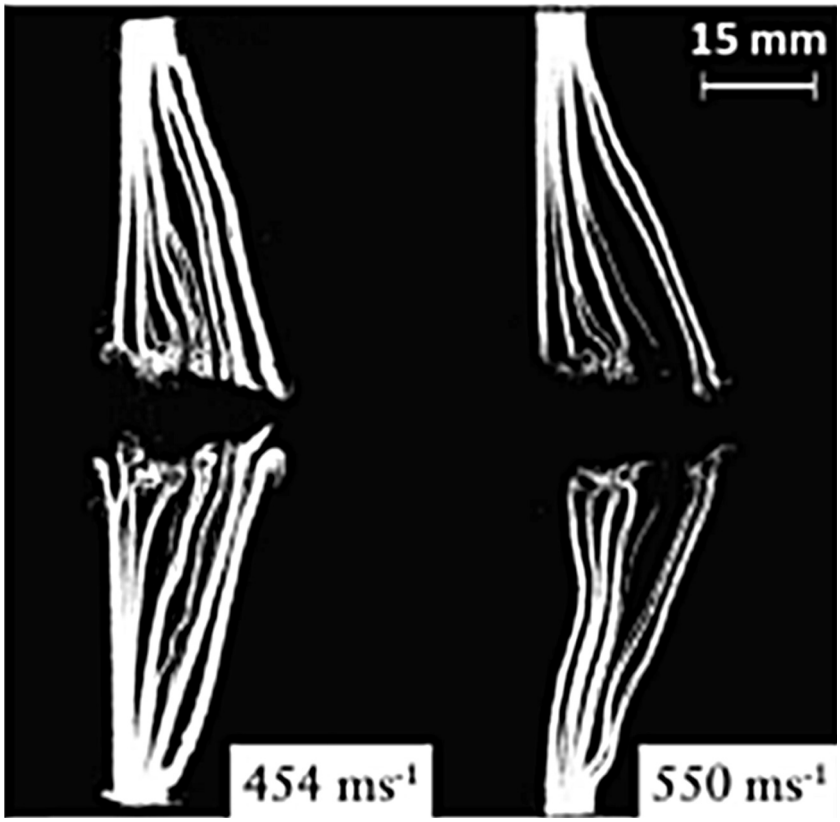

Fig. 4. From Karthikeyan et al. [10] – X-ray images of ballistic failure of a UHMWPE/polyurethane (Dyneema HB26) composite.

Porras et al. [31] measured mode II values. Both Grujicic et al. [13] and Porras et al. [31] found that UHMWPE composites exhibit much lower mode II values than some other composite types, such as carbon and *para*-aramids.

2.2.4. Mass of composite accelerated

Before target perforation or projectile stoppage, a semi-cone-shaped mass of composite material is accelerated [32,33]. The tip of the cone moves with the projectile and the cone base radius expands with time at the transverse wave speed. However, it has been observed that a projectile travels through UHMWPE composite layers in a progressive manner, causing the failed layers to delaminate extensively from the remaining intact portion (within the deformation cone zone) [8,10,29]. Once failed and delaminated from the intact portion of the composite, these layers are no longer subjected to acceleration. Therefore, at any given time, this model only takes into account the layers that haven't yet failed through shear or tension when determining the energy absorbed through acceleration of the composite mass. Fig. 6 depicts the region of the composite being accelerated.

The energy absorbed through acceleration of the composite mass can be described as the kinetic energy that is imparted to it. In a situation where the composite cone base can continue to grow, unimpeded by edges of a finite sized target, the energy can be described as:

For $r_T \leqslant \frac{L_T}{2}$ in a finite sized target, or when the target size is infinite:

$$E_{Acceleration} = \sum \frac{mass_i\, velocity_i^2}{2} = .5A_{ql}\pi \sum \left(r_{T,i}^2 - r_{T,i-1}^2\right) \cdot \left(h_c - N_{SP,i}h_L - N_{T,i}h_L\right)\rho_c v_i^2 \quad (18)$$

where L_T is the length of the target edge and ρ_c is the composite density. In certain situations, when the target is considered to be finite and the transverse wave reaches its edge before perforation, the mass of composite accelerated is also affected by the size and shape of the target and clamps. If the target or clamp configuration is square and the base of the deformation cone reaches the edge, it can no longer be considered a circular shape. As the base continues to spread, it transforms into a square shape as shown in Fig. 7.

Therefore, in this scenario when the base of the deformation cone reaches the edge of the target, but has not yet reached the outer corners, the area of the accelerated material transitions to a square shape that is bound by the target edges. To accomplish the calculation of this new area as it evolves involves subtracting the areas of the deformation cone base that extend beyond the plate edges. The intersections of the cone base and the plate edge form an angle, λ, which continues to grow larger until it reaches its maximum of 90 degrees. It can be shown that the area of the deformation cone base when it has reached the edge of the target, but has yet to fully cover the target, is:

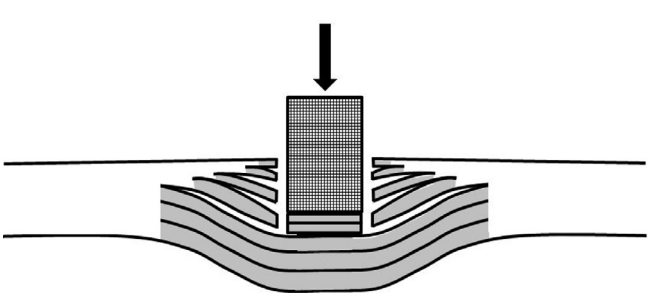

Fig. 6. Description of the mass of composite accelerated (dark area).

$$A_{b,i} = \pi A_{ql} r_{T,i}^2 - 2\left(\frac{\pi r_{T,i}^2}{90} \cdot \cos^{-1}\left(\frac{L_T}{2r_{T,i}}\right) - L_T\sqrt{r_{T,i}^2 - \left(\frac{L_T}{2}\right)^2}\right) \quad (19)$$

And subsequently, within this region, the additional energy absorbed by accelerating this mass is:

For $\frac{L_T}{2} < r_T \leqslant \frac{L_T}{\sqrt{2}}$ for a finite sized square target:

$$E_{Acceleration} = .5\sum \left(A_{b,i} - A_{b,i-1}\right) \cdot \left(h_c - N_{SP,i}h_L - N_{T,i}h_L\right)\rho_c v_i^2 \quad (20)$$

2.2.5. Shear plugging

During impact of the projectile onto the composite plate, shear stress is developed around the projectile perimeter. The plugging stress can be expressed as:

$$\sigma_{SP,i} = Force_i / ShearArea_i = Fp_i / \left(\pi d_p \left(h_c - N_{SP,i}h_L - N_{T,i}h_L\right)\right) \quad (21)$$

where *Fp* is the contact force resulting from the mass of the projectile along with any sheared composite material at its tip. This can be expressed as:

$$Fp_i = \left(m_p + \rho_c(N_T + N_{SP})h_L\left(\frac{\pi d_P^2}{4}\right)\right)dc_i \quad (22)$$

If this stress is greater than the through-thickness shear strength of the composite material, failure occurs by plugging. The energy absorbed by shear plugging can be expressed as the product of the composite shear strength, the area under shear stress and the distance sheared [17]:

If $\sigma_{SP} > S_{SP}$

$$E_{Shear} = \sum S_{SP}\, \pi\, d_p\, S_{P,i}^2 \quad (23)$$

where S_{SP} is the composite through-thickness shear strength. The through-thickness shear strength value used in the model came from experimental data presented by Umberger and Case [34] in which shear strengths of UHMWPE composites were measured with circular punch fixtures that either allowed composite back face curvature to occur naturally or prevented it.

2.2.6. Matrix cracking

As described by Naik et al. [17], matrix cracking also follows a quasi-lemniscate shape within the zone of composite deformation. It occurs in the region of the composite where the tensile strain is greater than the failure strain of the matrix. Therefore the damage radius for matrix cracking is determined by the magnitude and spacial profile of the overall level of composite tensile strain. As the strain wave propagates outward, the matrix fails in tension until the overall strain diminishes to less than the matrix failure strain. Additionally, due to composite void content, fiber/volume ratios, and transitions in failure mode through the event, the matrix may not completely crack during failure. Thus considering the mode I strain energy release rate, G_I, and percentage of total matrix cracking, P_m, as used by Naik et al. [25], the total energy absorbed through matrix cracking is:

If $\varepsilon_t > \varepsilon_m$

$$E_{Cracking} = \sum 2P_m\, A_{ql}\, \pi\, r_{p,i}\, G_I\, N_{L,i}\, h_L \quad (24)$$

where N_L is the number of layers remaining that have not failed. A value of .75 was applied for P_m. As described above, the progressive failure of composite layers as the projectile proceeds through the target leads to delamination that separates the failed layers from the remaining intact portion of the composite that is left to resist the projectile motion. Therefore, the region of matrix cracking only continues to grow within the intact portion of the composite.

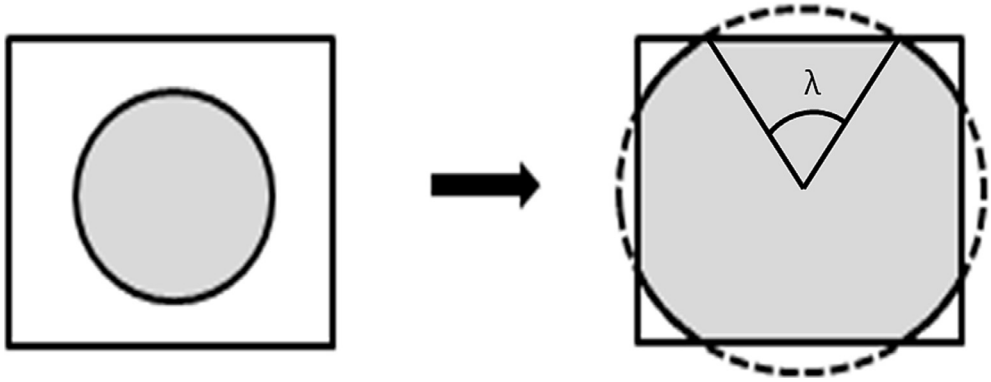

Fig. 7. Description of cone base change of shape when reaching target edges.

3. Comparison to experimental results

The model was compared to experimental results from four different researchers for ballistic limit and residual velocity after failure. The published experimental data included variations in composite thickness, projectile mass, projectile shape and projectile diameter. The model provided acceptable agreement for all experimental results it was evaluated against. Table 1 describes the experimental parameters, as well as the experimental and calculated ballistic limits. Fig. 8 plots the experimental and predicted ballistic limits for the various tests.

The material properties used ballistic limit comparisons in the model and their sources are shown in Table 2.

For sample number 7 from Table 1, Nuygen et al. [37] also provided residual velocity. Thus it was considered, as well as results by Chocron et al. [18]. Chocron et al. used a different UHMWPE composite type (Dyneema HB80®, based on the SK76 fiber), which possesses slightly different properties than those shown in Table 2. Thus, for consistency, the different properties reported by Chocron et al. [18] (fiber volume fraction 84%, fiber density 980 kg/m^3, layer thickness 40 μm) were used. And as Chocron et al. pointed out, each layer of material contains 4 plies: $[0/90]_2$. Thus, h_L as used in the model is actually the thickness of a single ply. Fig. 9 provides the residual velocity comparisons. It can be see that the model underpredicted Nguyen et al.'s results and overpredicted Chocron et al.'s results somewhat, but still provided reasonable approximations for the expected residual velocities. With respect to the results of Nuygen et al. [37] in particular, the shape of the curve appears accurate.

4. Example model output

Two cases for model output are presented, with the goal of providing example output that is representative of the range of properties found in the experimental results that were used for model validation.

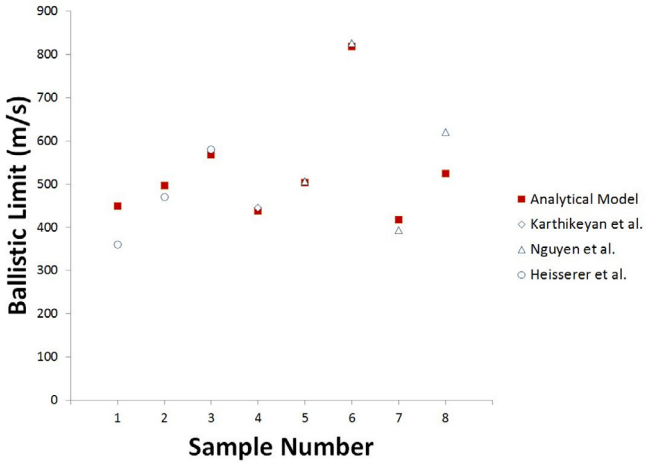

Fig. 8. Comparison of predicted ballistic limits with experimental results from Karthikeyan et al. [10], Nguyen et al. [11], and Heisserer et al. [35].

4.1. Case 1 – Thin Target/Low Mass Projectile/Small Diameter Projectile

The first case presented uses the same parameters used by Heisserer et al. [35] for a thin target tested in their experimental work. Of the experiments evaluated herein, this represented the smallest projectile mass, smallest projectile diameter, and a thin target. The values used in the model are shown in Tables 1 and 2. Fig. 10 compares the kinetic energy of the projectile to the various energy absorption mechanisms over the duration of the impact event.

Table 1
Experimental and predicted ballistic limits and parameters.

Sample No.	Target Thickness (mm)	Projectile Mass (g)	Projectile Diameter (mm)	Projectile Shape	Experimental Ballistic Limit (m/s)	Predicted Ballistic Limit (m/s)	Experimental Data Source
1	2.5	1.1	5.46	MIL-DTL-46593B FSP	360	450	Heisserer et al. [35]
2	4	1.1	5.46	MIL-DTL-46593B FSP	470	496	Heisserer et al. [35]
3	6	1.1	5.46	MIL-DTL-46593B FSP	580	567	Heisserer et al. [35]
4	6	8.3	12.7	Sphere	445	438	Karthikeyan et al. [10]
5	9.1	13.4	12.7	MIL-DTL-46593B FSP	506	503	Nguyen et al. [11]
6	20	13.4	12.7	MIL-DTL-46593B FSP	826	818	Nguyen et al. [11]
7	10	53.8	20	MIL-DTL-46593B FSP	394	417	Nguyen et al. [11]
8	20	53.8	20	MIL-DTL-46593B FSP	620	525	Nguyen et al. [11]

Table 2
Material properties used in the model and their sources.

Material Property	Value	Source
Fiber density, ρ_f, (kg/m3)	970	[6]
Fiber Volume fraction, V_f	.82	[10]
Fiber diameter, d_f, (μm)	17	[6,10,14]
Fiber dynamic tensile strength, $\sigma_{f,f}$, (MPa)	2500	[1,6]
Fiber dynamic strain, $\varepsilon_{f,f}$, (%)	2.0	[6]
Fiber dynamic modulus, E_f, (GPa)	130	[6]
Matrix density, ρ_m, (kg/m3)	1140	[36]
Matrix dynamic tensile strength, $\sigma_{m,f}$, (MPa)	100	[36]
Matrix dynamic strain, $\varepsilon_{m,f}$, (%)	1.3	[36]
Matrix dynamic modulus, E_m, (MPa)	77	[36]
Composite through-thickness shear strength, S_{SP}, (MPa)	220	[34]
Composite layer thickness, h_L, (μm)	60	[11,14]
Strain energy release rate, mode I, G_I, (J/m^2)	493	[13,30]
Strain energy release rate, mode II, G_{II}, (J/m^2)	38	[13,31]

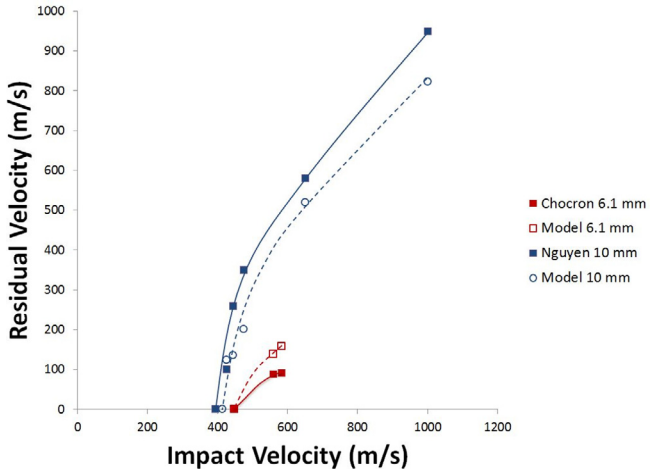

Fig. 9. Comparison of residual velocity between the model output and experimental data provided by Nguyen et al. [11,37] and Chocron et al. [18]. The experiment by Nguyen et al. was for a 10 mm thickness Dyneema HB26® impacted by a 20 mm FSP. The data from Chocron et al. was for 6.1 mm thickness Dyneema HB80® panel impacted by a 7.62 mm FSP.

The value for matrix cracking energy absorption was minimal and is therefore not shown in the plot.

It can be seen that the energy absorbed by tensile strain and acceleration of the composite cone both increase rapidly at first and then slow down over the duration of the event. Conversely, the delamination energy absorption increases in a steadier manner until failure. This is primarily because, as can be seen in Eqs. (14) and (18), both the tensile strain energy and the cone mass acceleration energy depend on a power of the velocity, as well as the volume of the composite involved. Both of these energy absorption mechanisms rise quickly in the beginning when the velocity is high and fall off as the projectile slows down and layers fail, reducing the volume of composite still acting to resist the projectile. The delamination energy, on the other hand, is not as dependent on the velocity and is primarily a function of the area of the composite failure cone and the number of interfaces in the remaining thickness (Eq. (17)). Although the number of interfaces decreases as layers fail, the delamination area grows quickly as the deformation cone diameter increases. Finally, the energy absorbed by shear failure was much smaller in magnitude than the other types. It increased slightly in the beginning of the event, but had ceased by 11 μs.

Fig. 11 shows the velocity profile for the projectile at impact velocities just below and above the ballistic limit (496 m/s vs. 497 m/s) for this case.

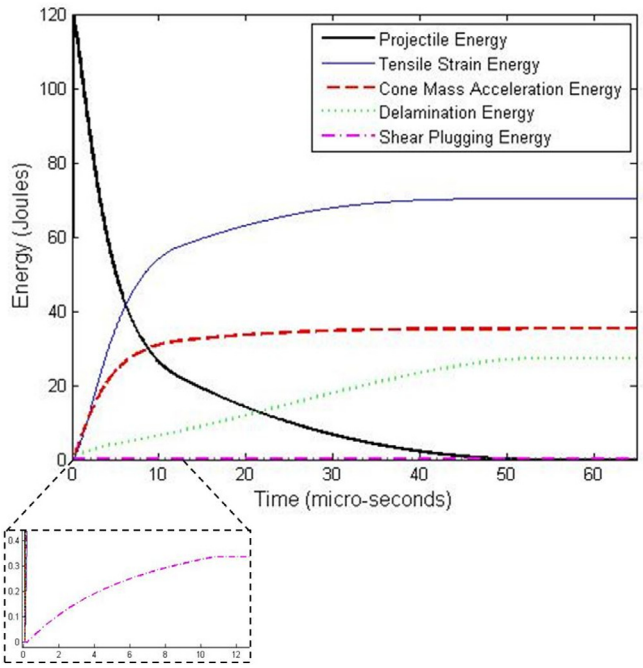

Fig. 10. Energy absorption for Case 1 – Thin Target/Low Mass Projectile/Small Diameter Projectile.

It can be seen that at just below the ballistic limit, the projectile velocity reduces to zero, but at just over the ballistic limit, there is a certain residual exit velocity (in this case 21.78 m/s).

4.2. Case 2 – Thick Target/High Mass Projectile/Large Diameter Projectile

In contrast to Case 1, Case 2 provides model results for the thickest target evaluated, with the largest projectile (mass and diameter). The parameters were taken from Nguyen et al., which are described in Table 1. Fig. 12 compares the kinetic energy of the projectile to the various energy absorption mechanisms over the duration of the impact event in this case. Again, the energy absorbed through matrix cracking was minimal and is therefore not shown in the plot.

The energy absorption characteristics were similar for both the thick and thin composites. Tensile strain was the primary energy absorber, followed by cone mass acceleration and delamination. Very little shear or matrix cracking failure was calculated in either case. The primary differences between Case 1 and Case 2 were the overall energy levels and the duration of the impact event. The larger projectile of Case 2 started with much more kinetic energy and the composite consequently absorbed more energy in all three major energy absorption mechanisms. And while the impact duration only lasted for 52 μs for Case 1 at the ballistic limit, it took 245 μs for full energy absorption in Case 2. Although the projectile kinetic energy was absorbed at a faster rate by the thicker composite (Case 2) in the beginning of the event, the absorption slowed down considerably and dragged out for a longer time period. This is due to the reduction of the composite thickness that acted upon the projectile as time went on. As the projectile penetrated the target, it failed layer by layer and near the end of the event, the number of active layers had been reduced significantly. Having only a few layers left near the end of the event, energy absorption was slower for the larger mass projectile in Case 2.

Similar to Case 1, it can also be seen that in Case 2, a small residual velocity remains when the impact velocity is slightly over the ballistic limit. Fig. 13 shows the velocity profiles for Case 2 with

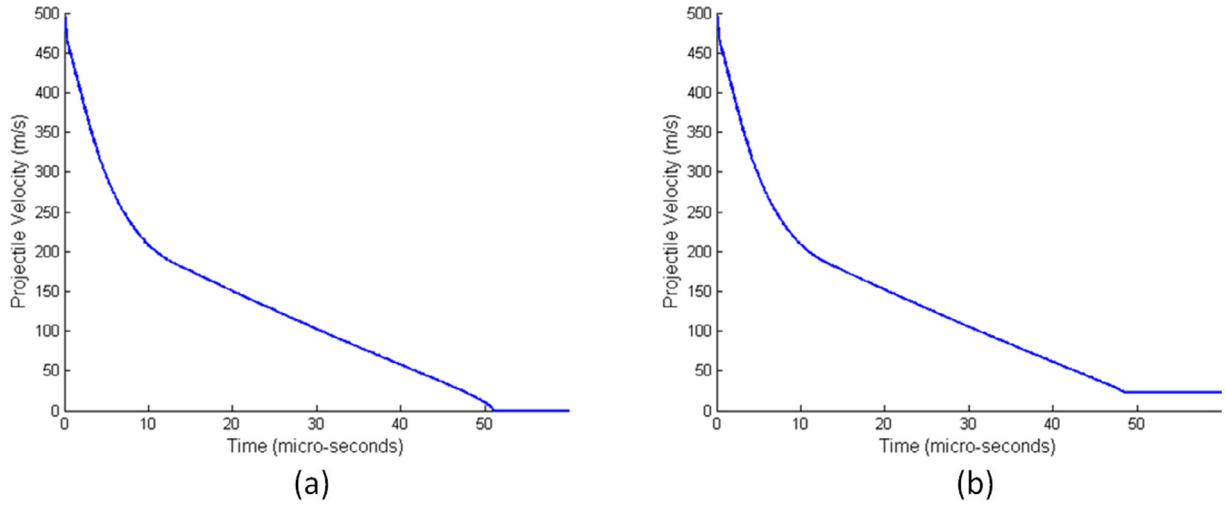

Fig. 11. Case 1 projectile velocity profile at impact velocities just below and above the ballistic limit (496 m/s vs. 497 m/s).

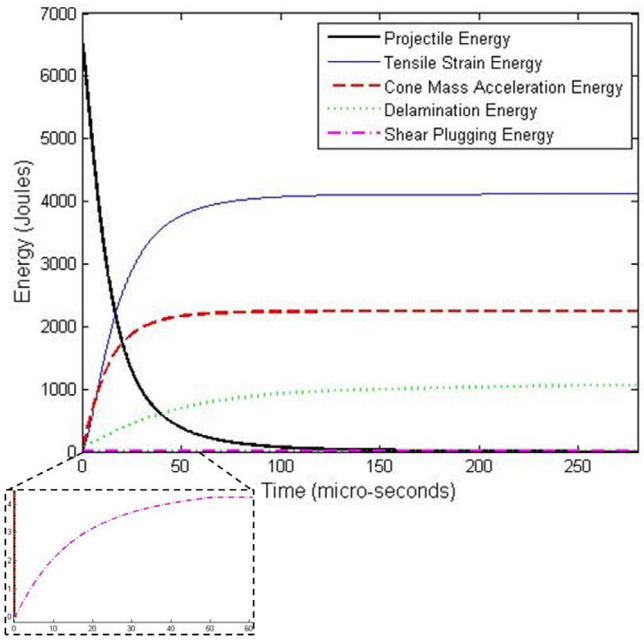

Fig. 12. Energy absorption for Case 2 – Thick Target/High Mass Projectile/Large Diameter Projectile.

impact velocities just below and above the ballistic limit (526 m/s vs. 527 m/s). The residual exit velocity for this example was 9.6 m/s.

There were two specific changes that occurred in the model at the ballistic limit: (1) the projectile was left with a residual exit velocity as shown in Figs. 11 and 13, and (2) the calculated failure distance of the composite reached the full target thickness. This can be seen in Fig. 14. At a velocity just below the ballistic limit, all of the energy was absorbed just before the composite failed all the way through, but at a velocity slightly above the ballistic limit, the composite failed through before the projectile velocity was reduced to zero.

As previously described, the total failure distance of the composite is a combination of the shear and tensile failure distances. Fig. 15 breaks out the shear and tensile failure distances over time, for Case 2. In the early stages, the conditions are right for failure from either shear or tensile strain. However, at approximately 50 μs, the shear stress is no longer high enough to cause failure and only the failure from tensile strain continues. This behavior is in agreement with the failure observations of Nguyen et al. [11], Iremonger et al. [12], and Grujicic et al. [13]. As previously mentioned, failure from transverse tensile cracking on the back side was also considered, but was not found to play a significant role. It is important to note that when the conditions were right for failures from both shear and tensile strain, the failure of only one layer was allowed to occur. They were mutually exclusive and either one or the other causes the layer failure.

5. Discussion

An energy-based analytical model was presented to predict the failure of UHMWPE composites against ballistic impact. The primary energy absorption mechanisms were found to be, in decreasing order: tensile strain, acceleration of composite mass, delamination, and shear failure. This is not surprising, due to the properties of the UHMWPE fibers and matrix materials used in these composites. The exceptionally high fiber strength lends itself to considerable energy absorption through tensile strain and the typical matrix materials possess very high toughness that leads to high energy absorption through delamination.

The energy absorption benefits of tensile strain and mass acceleration were realized very quickly, while the energy absorption due to delamination increased at a steadier pace throughout the impact event. This can be explained by the dependence of these energy absorption mechanisms on the projectile velocity. Both the tensile strain and the mass acceleration depend on a higher power of the projectile velocity. Thus, when the velocity is high in the early stages of the event, energy absorption increases rapidly, but as the velocity diminishes, the energy absorption from these mechanisms levels off.

Delamination is also dependent on the projectile velocity, as it affects the transverse wave speed in the composite cone. This, in turn, determines the delamination area. However, the equation for the transverse wave speed (Eq. (8)) contains a square root term, which significantly reduces the influence of the projectile velocity. It should be noted, however, that all three primary energy absorption mechanisms are mitigated by through-thickness failure of the composite. As the failed number of layers increases, the volume of composite material participating in tensile strain, the mass being accelerated, and the number of interfaces being delaminated all decrease.

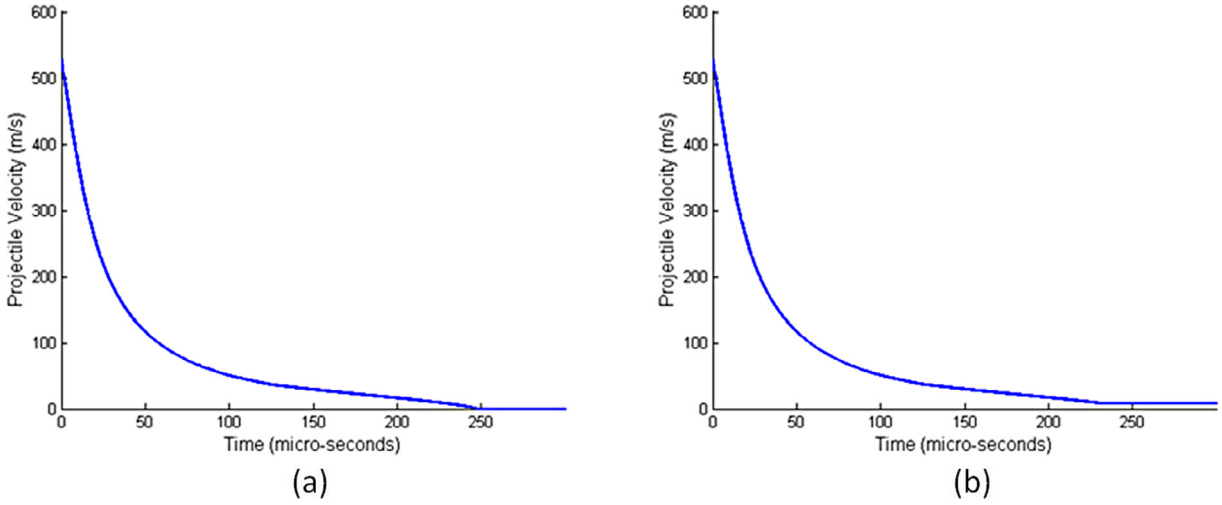

Fig. 13. Case 2 projectile velocity profile at impact velocities just below and above the ballistic limit (526 m/s vs. 527 m/s).

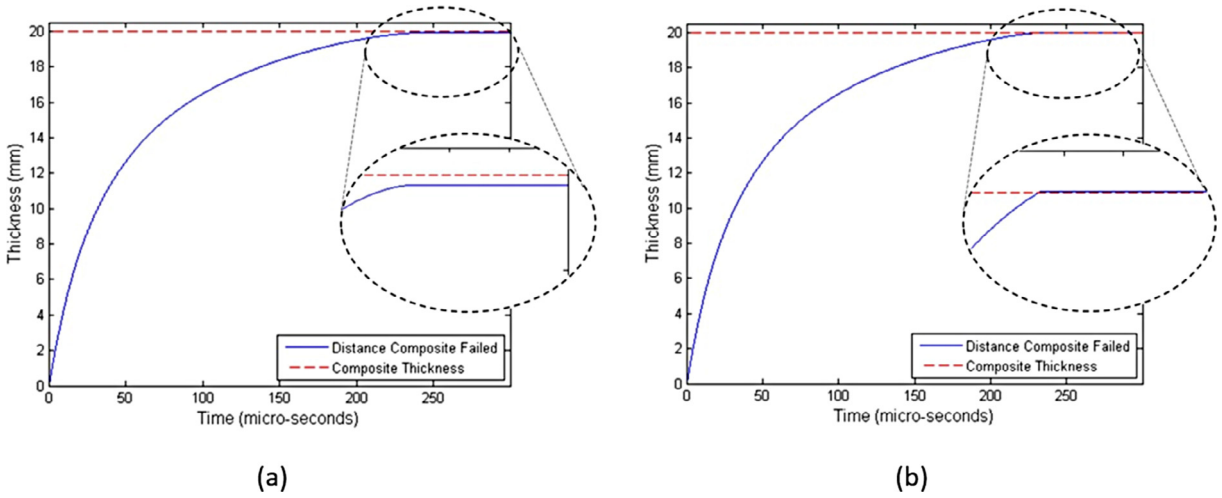

Fig. 14. Comparison of the composite through-thickness failure distance just below the ballistic limit (526 m/s) and just above (527 m/s) for case 2.

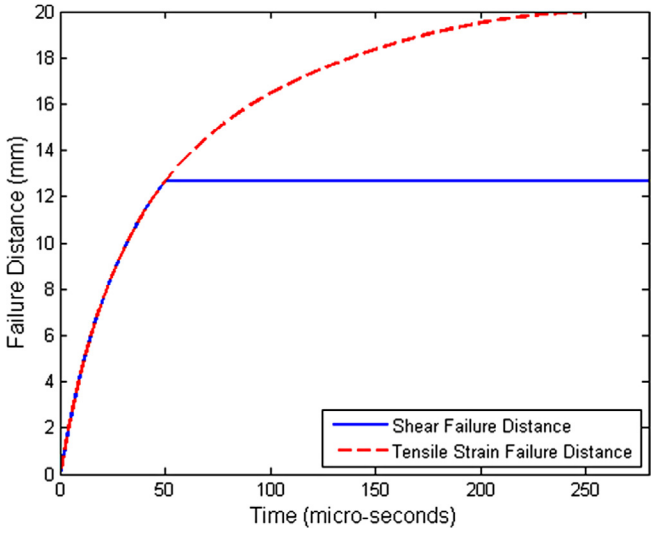

Fig. 15. Failure distances of each failure type (shear and tensile strain). Transverse tensile cracking was not observed in this case.

The energy absorption contribution from shear failure was small, and occurred only in the beginning of the events evaluated. This is in agreement with other researchers. Nguyen et al. [11] examined fiber failures through a failed UHMWPE composite, from the front to the back. They noted a change in the fiber failure morphology that suggested shear failure in the earlier layers of the composite and tensile failure in the latter ones. Iremonger et al. [12] also observed filament shearing in the early layers of failed UHMWPE composites, followed by delamination in the latter layers. The finite element model presented by Grujicic et al. [13] described the stages of failure of UHMWPE composites in order as 1) filament shearing; 2) delamination and debonding; and 3) extensive filament extension.

Although matrix cracking was also considered in the model, relatively little appreciable energy absorption or through-thickness failure was found to result from it in the cases considered. This is sensible, considering the properties of the matrix materials utilized in these types of composites. When compared to the energy required for straining the high-modulus fibers and accelerating the composite mass, the energy required for crack growth is relatively much smaller.

Another benefit of the UHMWPE fibers was found to be that they have a very high plastic wave speed, allowing the composite

cone to grow very rapidly after impact. The faster the composite deformation cone grows, the more rapidly the energy is absorbed and spread out, thereby minimizing high stresses that are localized at the projectile contact zone.

Through-thickness failure of individual layers was found to occur from both shear failure and tensile strain of the fibers beyond their ultimate limit. Although some bending strain was calculated in the back layers of the composite, it was never found to be high enough to cause transverse tensile cracking. The type of failure observed in the model supports the observations of Karthikeyan et al. [10] and O'Masta et al. [8] who observed progressive failure of UHMWPE composites (HB26 and HB50 Dyneema®) from front to back. The tensile strain used to determine failure in the current model was a combination of the strain that resulted from the formation of the composite cone and the additional strain from laminate compression, which occurred directly under the projectile. Shear failure was only found to occur in the beginning layers of the target, which is in agreement with Nguyen et al. [11], Iremonger et al. [12], and Grujicic et al. [13] Tensile strain failure also occurred in the early stages of impact but continued deeper and played a larger role as the composite thickness and projectile mass was increased. This is reasonable because both of these variables lead to increased compressive stress under the projectile, which as Woodward et al. [27] and Attwood et al. [14] contended, leads to increased tensile failures.

The model was found to agree well with published experimental data for UHMWPE ballistic tests in regard to ballistic limit. Experimental data was collected that represented a range of parameters, including target thickness, projectile mass and projectile diameter. Although the model agreement was excellent for all of the parameters considered, more error was noticed with the thinnest and thickest targets than with the middle thicknesses. This suggests that the thickness ranges considered might represent the appropriate range of application for this model. Very thin or thick targets may require particular modeling approaches that consider their unique characteristics.

6. Conclusions

UHMWPE fibers (Dyneema, Spectra) possess some of the most impressive properties available for ballistic armor. They offer extremely high tensile strength, stiffness, and strain to failure, while having the lowest density of the high-performance fibers considered. They also offer exceptionally high plastic wave speeds, allowing for rapid energy absorption and dispersion.

This paper has presented an analytical model to aid in the design and use of these materials in ballistic armor applications. The model predicts ballistic limit, residual velocity, through-thickness failure distance, and energy absorption. Reasonable agreement was attained with published experimental data. Tensile strain, acceleration of the composite mass and delamination were found to be the primary mechanisms of energy absorption, while matrix cracking played a much smaller role. Failure was found to occur from front to back, beginning with shear plugging, but then transitioning to tensile failure. Both compression under the projectile and formation of the failure cone led to tensile strain.

Acknowledgements

This work was sponsored by the Combatting Terrorism Technical Support Office (CTTSO) Technical Support Working Group (TSWG). The author would like to thank the program manager, Amanda Toman, and program analyst, Brady Russell. The views expressed herein are those of the author and do not reflect the official policy or position of the Department of the Navy, Department of Defense, or any agency of the United States Government.

References

[1] Huang W, Wang Y, Xia Y. Statistical dynamic tensile strength of UHMWPE-fibers. Polym 2004;45:3729–34.
[2] Koh ACP, Shim VPW, Tan VBC. Dynamic behaviour of UHMWPE yarns and addressing impedance mismatch effects of specimen clamps. Int J Impact Eng 2010;37:324–32.
[3] Koh C, Shim V, Tan V, Tan B. Response of a high-strength flexible laminate to dynamic tension. Int J Impact Eng 2008;35:559–68.
[4] Zhou Y, Wang Y, Xia Y, Jeelani S. Tensile behavior of carbon fiber bundles at different strain rates. Mater Lett 2010;64:246–8.
[5] Wang Y, Xia YM. Experimental and theoretical study on the strain rate and temperature dependence of mechanical behaviour of Kevlar fibre. Compos A 1999;30:1251–7.
[6] Russell BP, Karthikeyan K, Deshpande VS, Fleck NA. The high strain rate response of Ultra High Molecular-weight Polyethylene: from fibre to laminate. Int J Impact Eng 2013;60:1–9.
[7] Toyobo Co, PBO Fiber Zylon Technical Information Sheet F0739K(2005.6).
[8] O'Masta MR, Deshpande VS, Wadley HNG. Mechanisms of projectile penetration in Dyneema ® encapsulated aluminum structures. Int J Impact Eng 2014;74:16–35.
[9] Jalalvand M, Wisnom MR, Hosseini-Toudeshky H, Mohammadi B. Experimental and numerical study of oblique transverse cracking in cross-ply laminates under tension. Compos: Part A 2014;67:140–8.
[10] Karthikeyan K, Russell BP, Fleck NA, Wadley HNG, Deshpande VS. The effect of shear strength on the ballistic response of laminated composite plates. European J Mech A/Solids 2013;42:35–53.
[11] Nguyen LH, Ryan S, Cimpoeru SJ, Mourtitz AP, Orifici AC. The effect of target thickness on the ballistic performance of ultra high molecular weight polyethylene composites. Int J Impact Eng 2015;75:174–83.
[12] Iremonger MJ. Polyethylene composites for protection against high velocity small arms bullets. Proc. 18th International Symposium on Ballistics, San Antonio, 15–19 November 1999. p. 946.
[13] Grujicic M, Glomski PS, He T, Arakere G, Bell WC, Cheeseman BA. Material modeling and ballistic-resistance analysis of armor-grade composites reinforced with high-performance fibers. J Mater Eng Perform 2009;18:1169–82.
[14] Attwood JP, Khaderi SN, Karthikeyan K, Fleck NA, O'Masta MR, Wadley HNG, et al. The out-of-plane compressive response of Dyneema composites. J Mech Phys Solids 2014;70:200–26.
[15] Smith JC, McCrackin FL, Schiefer HF. Stress-strain relationships in yarns subjected to rapid impact loading: 5. Wave propagation in long textile yarns impacted transversely. J Res Natl Bureau Standards 1958;60:517–34.
[16] Roylance DK, Wilde AF, Tocci GC. Ballistic impact of textile structures. Army Materials and Mechanics Research Center, Report AMMRC TR 73–8, Feb. 1973.
[17] Naik NK, Shrirao P, Reddy BCK. Ballistic impact behavior of woven fabric composites: Formulation. Int J Impact Eng 2006;32:1521–52.
[18] Chocron S, Nicholls AE, Brill A, Malka A, Namir T, Havazelet D, et al. Modeling unidirectional composites by bundling fibers into strips with experimental determination of shear and compression properties at high pressures. Compos Sci Technol 2014;101:32–40.
[19] Hudspeth M, Nie X, Chen W. Dynamic failure of Dyneema SK76 single fibers under biaxial shear/tension. Polymer 2012;53:5568–74.
[20] Utomo BDH, Ernst LJ. Detailed modeling of projectile impact on Dyneema composite using dynamic properties. J Solid Mech Mater Eng 2008;2 (6):707–17.
[21] Harris B. Engineering composite materials. London: The Institute of Materials; 1999. p. 44–6.
[22] Bunsell AR, Renard J. Fundamentals of fibre reinforced composite materials. CRC Press; 2005. p. 244–7.
[23] Krenchel H. Fibre Reinforcement. Copenhagen: Akademisk Forlag; 1964.
[24] Gupta KM. Engineering materials: research, applications and advances. CRC Press; 2014. p. 125–7.
[25] Naik NK, Satyanarayana Reddy K. Delaminated woven fabric composite plates under transverse quasi-static loading: experimental studies. J Reinf Plast Comp 2002;21:869–77.
[26] Wu E, Chang L. Woven glass/epoxy laminates subject to projectile impact. Int J Impact Eng 1995;16:607–19.
[27] Woodward RL, Egglestone GT, Baxter BJ, Challis K. Resistance to penetration and compression of fiber-reinforced composite mateirals. J Appl Mech 1994;4 (3):329–41.
[28] Gellert EP, Cimpoeru SJ, Woodward RL. A study of the effect of target thickness on the ballistic perforation of glass-fibre-reinforced plastic composites. Int J Impact Eng 2000;24:445–56.
[29] Deka LJ, Bartus SD, Vaidya UK. Damage evolution and energy absorption of FRP plates subjected to ballistic impact using a numerical model. In: 9th International LS-DYNA Users Conference, Impact Analysis, Dearborn, MI, June 2006, p. 4–49 – 4–60.
[30] Lassig T, Nolte F, Riedel W, May M. An assessment of experimental techniques for measuring the mode I fracture toughness of UHMW-PE composites. In: 17th European Conference on Composite Materials, Munich, Germany, 26–30 June 2016. p. 1–8.

[31] Porras A, Tellez, J, Casas-Rodriguiez, JP. Delamination toughness of ultra high molecular weight polyethylene (UHMWPE) composites. In: DYMAT 2012–10th International Conference on the Mechanical and Physical Behaviour of Materials under Dynamic Loading, Freiburg, Germany, 2012. p. 1–4.
[32] Morye SS, Hine PJ, Duckett RA, Carr DJ, Ward IM. Modelling of the energy absorption by polymer composites upon ballistic impact. Compos Sci Technol 2000;60:2631–42.
[33] Zhu G, Goldsmith W, Dharan CK. Penetration of laminated Kevlar by projectiles—I. experimental investigation. Int J Solids Struct 1992;29:399–419.
[34] Umberger, PD, Case, SW. Through thickness shear and membrane behavior of UHMWPE composites. In: Proceedings of the 42nd Annual International SAMPE Technical Conference, Society for the Advancement of Material and Process Engineering, Covina, CA, January 2010.
[35] Heisserer U, van der Werff H. The relation between Dyneema fiber properties and ballistic protection performance of its fiber composites. In: 15th International Conference on Deformation, Yield and Fracture of Polymers, Netherlands, 1–5 April 2012. p. 242.
[36] Yi J, Boyce MC, Balizer E, Lee G. Large Deformation Rate-Dependent Stress-Strain Behavior of Polyurea and Polyurethane. Polymer 2006;47:319–29.
[37] Nguyen LH, Lassig TR, Ryan S, Riedel W, Mouritz AP, Orifici AC. A methodology for hydrocode analysis of ultra-high molecular weight polyethylene composite under ballistic impact. Compos: Part A 2016;84:224–35.